Available online at www.HighTechJournal.org

HighTech and Innovation Journal

ISSN: 2723-9535

Vol. 7, No. 1, March, 2026

Style Conversion of Zhuang Brocade Patterns Based on Low Rank Adaptive and Deep Learning

Li'na Zhao [1*], Xiaoxuan Nie [1]

[1] *College of Beauty Art, Tongmyong University, Busan, 48520, Korea.*

Received 13 August 2025; Revised 03 January 2026; Accepted 08 January 2026; Published 01 March 2026

Abstract

As a key bearer of traditional Zhuang culture, Zhuang brocade patterns face challenges such as low design efficiency and a stylistic disconnect from modern demands. Therefore, this study innovatively proposes an integrated model that combines low rank adaptive fine-tuning, stable diffusion model, and generative adversarial network for intelligent pattern generation and style transformation. This model adopts an image-to-image method based on GAN for pattern generation, and introduces an improved synthesis and cascading transformation method to achieve differentiated style conversion of brocade patterns. In performance validation experiments, the model demonstrates clear clustering boundaries in complex pattern feature recognition, with a peak signal-to-noise ratio of 32.5 dB, an initial style transfer score of 78.3, and an average diversity index of 0.78. When processing 400 data samples, the model requires 1123 MB of memory and responds within 122 ms, significantly outperforming comparison models in both performance and efficiency. The results show that the model proposed in the study has advantages in the intelligent generation of Zhuang brocade patterns and style transfer generation quality, style adaptability and comprehensive use of resources. The research results provide an effective solution for intelligent pattern generation and modern style adaptation, with broader potential applications in protecting and innovating intangible cultural heritage.

Keywords: LoRA; Stable Diffusion; GAN; Style Transfer; Zhuang Brocade Patterns.

1. Introduction

As one of the four major brocades in China, Zhuang brocade carries the life wisdom and cultural memory of the Zhuang ancestors. It is not only a vital part of Chinese intangible cultural heritage but also a key material in modern design that blends tradition and innovation [1, 2]. However, in the digital era, Zhuang brocade patterns face challenges such as inefficient hand-drawn design and a stylistic gap between traditional aesthetics and modern tastes, which disconnect cultural value from market demand. Therefore, exploring intelligent generation and style transfer technologies for Zhuang brocade patterns has become essential to promoting the living inheritance of intangible culture [3, 4]. Existing technologies in ethnic pattern processing often struggle to capture distinctive features and tend to lose core cultural elements during the transfer process. The development of style transfer technology offers new possibilities to address these issues [5]. Many scholars have conducted extensive research on pattern generation and style transfer techniques. For instance, Mao Yang raised a method for transferring artistic text style by mapping complex textures and structures to achieve artistic expression, though it lacked attention to local visual features [6]. Zhang et al. proposed a novel art style conversion framework ArtBank to address the issue of existing art style conversion methods being unable to generate highly realistic stylized images. They also designed an implicit style prompt library and a spatial statistics

* Corresponding author: linazhaobb@outlook.com

https://doi.org/10.28991/HIJ-2026-07-01-012

based self-attention module. Qualitative and quantitative experiments have shown that the proposed method outperforms state-of-the-art art style conversion methods [7]. Yan et al. innovatively proposed a fashion attribute disentanglement Generative Adversarial Network (GAN) to assist fashion designers in automatically completing texture design, and proposed a texture exchange module to learn mixed texture codes to eliminate differences in features of different fashion items. The results showed that the mask learned perceptual image patch similarity of the proposed method improved by 0.006-0.446 [8]. Liu et al. considered site-specific magnetic resonance imaging coordination as a style transfer problem and used a fully unsupervised deep learning framework based on GAN for style transfer. The results indicate that the proposed style encoding model can coordinate magnetic resonance imaging [9]. Garg et al. proposed a steganography technique for reliable transmission of sensitive data, using neural style transfer algorithm to generate steganographic images and conditional GAN for de standardization. The results showed that the peak signal-to-noise ratio, structural similarity index, and visual information fidelity of the proposed method were 44.175 dB, 0.9958, and 0.954, respectively [10].

However, existing studies mainly focus on general visual scenarios and lack mechanisms for transferring the hierarchical features of Zhuang brocade. This limitation makes it difficult to adapt traditional and modern styles simultaneously. The emergence of Low-Rank Adaptation (LoRA) has provided a new path for lightweight customization of large models. LoRA reconstructs model weight increments through low-rank matrix decomposition, enabling nearly full fine-tuning effects by adjusting only a small number of parameters, which significantly reduces training costs. Wang et al. combined federated learning with LoRA to efficiently fine-tune large language models in wireless networks, validating its applicability in resource-limited settings [11]. Jin et al. put forward a derivative-free optimization method that further enhanced LoRA's efficiency in large language model tuning [12]. Imam et al. applied a confidence-maximization approach using LoRA to improve zero-shot generalization in vision-language models [13]. Becha et al. used LoRA to fine-tune large models and significantly improved cancer detection accuracy [14]. Lu et al. demonstrated through low-rank correlation learning that LoRA strengthens feature association in unsupervised domain adaptation [15]. These findings suggest that LoRA holds advantages in lightweight tuning and feature enhancement, providing technical support for addressing the challenge of capturing niche features in Zhuang brocade pattern generation.

In summary, although significant progress has been made in the field of general image style transfer in existing research, and the effectiveness of LoRA in lightweight adjustment and feature enhancement has been demonstrated. However, most existing methods are aimed at general visual scenes or specific functional requirements, lacking mechanisms for effectively identifying, maintaining, and transferring the hierarchical cultural features and semantic symbols unique to intangible cultural heritage. To fill this research gap, this study creatively integrates LoRA-based fine-tuning, GAN, and an improved style transfer algorithm to build a model for intelligent generation and style transfer. The model uses LoRA to fine-tune the Stable Diffusion 3 (SD3) model for enhanced capture of subtle features in Zhuang brocade, and incorporates the adversarial mechanism of GAN to correct detail deviations and achieve differentiated transfer of hierarchical features. This work aims to address issues of low design efficiency and poor style adaptability in Zhuang brocade patterns. The proposed model is expected to provide a technical framework for the digital inheritance of intangible cultural heritage and its application in modern design, promoting a deeper integration between traditional crafts and intelligent technology.

This study is structured in four parts. The first part is to build an intelligent generation method for Zhuang brocade patterns based on LoRA and a Zhuang brocade image generation model based on style conversion. The second part is to analyze the application effect of the proposed algorithm. The third part is a discussion of the research results and other related studies. The last part is a summary of the entire study.

2. Methods and Materials

2.1. Design of Intelligent Generation Method for Zhuang Brocade Patterns based on LoRA

Zhuang brocade patterns face practical challenges such as low design efficiency and a disconnection from market demands. SD3 is currently a leading open-source model in image generation, so this study adopts SD3 to generate novel Zhuang brocade patterns that align with modern aesthetics [16]. The general process of text-to-image generation is shown in Figure 1.

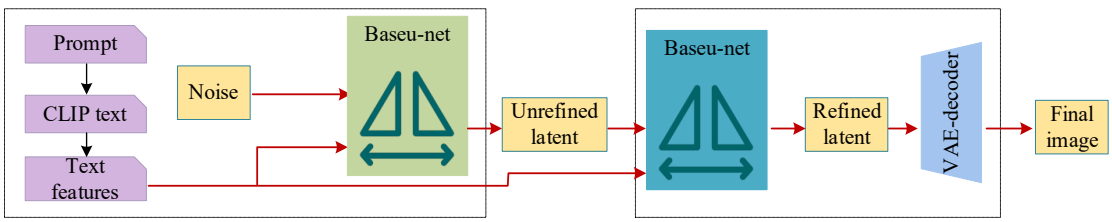

Figure 1. SD3 text-to-image generation process

In Figure 1, the core process of SD3 in text-driven image generation includes three stages: input of text and noise, feature refinement, and image decoding. The input text that describes image features is combined with random noise to generate optimized latent features. These features are refined through iterative optimization and then decoded into the final image. The hierarchical design of SD3's dual-feature generator improves the efficiency of converting text into images. The calculation of noise addition to spatial features in SD3 is shown in Equation 1 [17].

$$z_t = \sqrt{\alpha_t} z_0 + \sqrt{1-\alpha_t}\varepsilon \tag{1}$$

In Equation 1, z_t represents the potential noisy features at time step t, z_0 represents the features encoded from the original image, α_t is the cumulative noise coefficient, and ε denotes Gaussian noise. The reverse denoising process in SD3 is described by Equation 2.

$$z_{t-1} = \frac{1}{\sqrt{\alpha_t}}(z_t - \frac{1-\alpha_t}{\sqrt{1-\alpha_t}}\varepsilon') + \sigma_t z_t \tag{2}$$

In Equation 2, z_t represents the potential features after denoising at time step $t-1$, ε' is the predicted Gaussian noise, σ_t is the noise coefficient that controls the diversity of noise generation, and t represents the ongoing timestep. The decoding of the latent representation into a final image by the VAE is calculated using Equation 3.

$$x_0 = VAE - Decoder(z_0') \tag{3}$$

In Equation 3, x_0 represents the final generated pixel image, z_0' is the final result from reverse denoising in the diffusion model. The generated pixel image is obtained through encoding and decoding. Although SD3's 2 billion parameters support diverse Zhuang brocade pattern generation, its high memory usage (up to 24 GB) and complex computational processes lead to style deviation when generating niche features such as rhombus frameworks and bronze drum patterns. Therefore, it is necessary to enhance the extraction of artistic features and design a lightweight generation path [18, 19]. LoRA reconstructs model weight increments through low-rank matrix decomposition. In SD3, it only needs to fine-tune 1% of the parameters to achieve performance close to full fine-tuning [20]. This feature, which requires only minor adjustments to a few parameters, forms the foundation for the proposed model's good scalability. When applied to larger and more diverse datasets of intangible cultural heritage patterns, the advantages of LoRA will be even more significant. Unlike traditional full fine-tuning, which requires almost linear growth in computing resources and storage space, LoRA introduces a low-rank bypass matrix that is decoupled from the base model. This means that when extended to new cultural patterns, LoRA does not need to replicate the entire SD3 base model, but only needs to train a lightweight LoRA adapter for each new pattern to achieve "one to many" cultural feature generation on a single base model. The increase in computation and memory overhead is only related to the size of low rank matrices and the number of new tasks, making it feasible and efficient to integrate large-scale and diverse datasets. Therefore, this framework is not only applicable to Zhuang ethnic brocade, but its design itself is a lightweight and intensive solution that can be efficiently extended to various cultural heritages. Figure 2 shows the process of parameter optimization using LoRA.

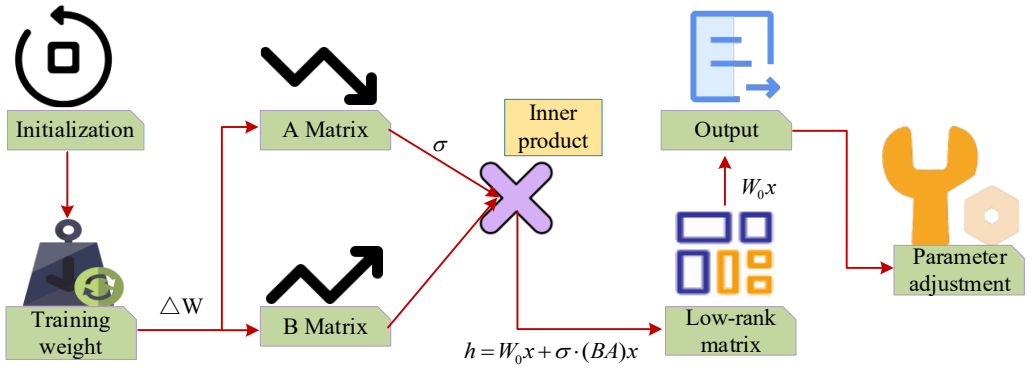

Figure 2. LoRA parameter optimization process

In Figure 2, LoRA achieves lightweight and precise fine-tuning through a process consisting of initialization and training, low-rank decomposition, inner product fusion, and parameter iteration. The initialization and training stage generates weight increments for Zhuang brocade features. These increments are then decomposed into input and output projections of low-rank matrices. Inner product operations between high- and low-dimensional matrices generate output features with low-rank constraints. The core idea of LoRA is to decompose the update of the original weight matrix into the product of two low-rank matrices, as shown in Equation 4 [21].

$$W = A \cdot B \tag{4}$$

In Equation 4, W is the original weight matrix of the pre-trained model, A is the dimensionality-reduction matrix that projects high-dimensional data into a low-rank space, and B is the upscaling matrix that restores the original dimensions. During SD3 training, LoRA introduces incremental updates via a bypass path, calculated as shown in Equation 5.

$$h = W_0 x + \sigma \cdot (BA)x \tag{5}$$

In Equation 5, h is the output of the layer, $W_0 x$ is the output from the frozen part of the original model, and σ is the scaling factor for the increment and rank, used to balance the contribution of the update. Although LoRA improves the efficiency of generating Zhuang brocade images using SD3, the resulting images may still contain blurred details and occasional structural deviations. GAN uses a dynamic game between generator and discriminator to mine latent feature distributions from imperfect training data. Through gradient feedback from the discriminator, the generation logic is refined iteratively. This adversarial process enhances detail accuracy and structural coherence, allowing the model to generate stylistically consistent images that outperform the flawed data [22]. Therefore, this study uses SD3-generated images as the training set for GAN and builds an image-to-image intelligent generation method for Zhuang brocade patterns, named SD3-GAN, to produce images with clearer details and more diverse patterns. The overall process is shown in Figure 3.

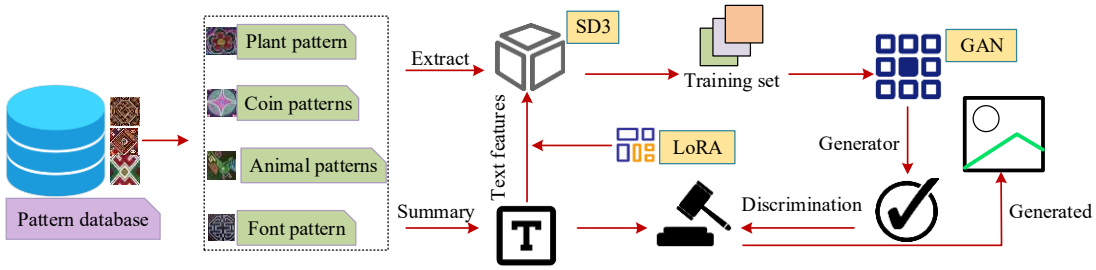

Figure 3. SD3-GAN intelligent image generation process

As shown in Figure 3, SD3-GAN addresses blurred details and structural deviations in SD3-generated images through an optimized image-to-image generation process. First, SD3-GAN extracts visual features of plants, geometry, animals, and fonts from the Zhuang brocade pattern library and summarizes the related text descriptions. Then, SD3 combines these features and texts to generate initial patterns with defects. These serve as training data for GAN, and the generator iteratively improves the images to produce Zhuang brocade patterns with refined details, consistent styles, and diverse structures. After training is complete, the generator's optimal parameters are determined using Equation 6.

$$\theta_{best} = \arg\max_{\theta} L = \arg\max \int_x P_{date}(x) \log \frac{P_g(x,\theta)}{P_{date}(x)} dx \tag{6}$$

In Equation 6, θ_{best} represents the optimal parameters of the generator, θ is a random parameter, L is the likelihood function that evaluates SD3-GAN's parameter performance, P_{date} represents the distribution of real image features, and P_g is the distribution of features generated by parameter θ. The similarity between generated and real data is then evaluated by Kullback-Leibler Divergence (KL), calculated in Equation 7.

$$KL(P \| Q) = \int P(x) \log \frac{P(x)}{Q(x)} dx \tag{7}$$

In Equation 7, $KL(P\|Q)$ represents divergence from KL, $P(x)$ and $Q(x)$ are the probability distributions of two continuous random variables in the generated and real images, respectively. A larger KL value indicates lower similarity. When $P(x) = Q(x)$, the KL divergence becomes zero, meaning the generated and real data are completely identical. The expression for the optimal parameters of SD3-GAN in this case is shown in Equation 8.

$$\theta_{best} = \arg\min_{\theta} KL(P_{date} \| P_g) \tag{8}$$

In Equation 8, when KL divergence is zero, the quality of the generated image is at its best.

2.2. Construction of Zhuang Brocade Image Generation Model with Style Transfer

Although SD3-GAN generates Zhuang brocade patterns with cultural features, there remains a semantic gap between the generated results and actual product design scenarios in terms of style adaptability [23]. The pattern structure, color

tone, or composition logic often cannot directly match the functional and aesthetic needs of modern products. Therefore, it is necessary to apply style transfer technology to semantically reconstruct the generated content. This allows the model to retain traditional cultural elements while adapting the patterns to various design contexts, such as clothing, home decor, and cultural products. Photographic Image Synthesis with Cascaded Transformations (PhotoWCT) is a deep learning-based image style transfer algorithm. It transforms features by matching the covariance of content images to that of style images, thereby preserving structural authenticity and visual coherence [24]. Based on this, the study improves upon PhotoWCT to develop a new algorithm for Zhuang brocade image style transfer. Style transformation should not only maintain visual consistency, but also respect the cultural semantics of the original patterns. Therefore, this study introduces a semantic perception module in the process of style transfer, which annotates and protects symbolic elements in patterns to ensure that these key cultural symbols are not distorted or lost during the style transfer process. This semantic perception module is implemented through a Contrastive Language Image Pre-training (CLIP) model. Specifically, a database is first built containing key symbolic symbols of Zhuang ethnic patterns and their textual descriptions. Before style transfer, use CLIP's image encoder to identify and segment these key cultural symbols in the content image, generating a semantic mask. In the loss function of AM-PWCT, an additional semantic consistency constraint (Semantic Consistency Loss) is introduced for the masked region, which calculates the cosine similarity between the generated image and the content image in the CLIP feature space to ensure that the core form and cultural semantics of these symbolic elements are preserved during the style transition process. The structure of PhotoWCT is shown in Figure 4.

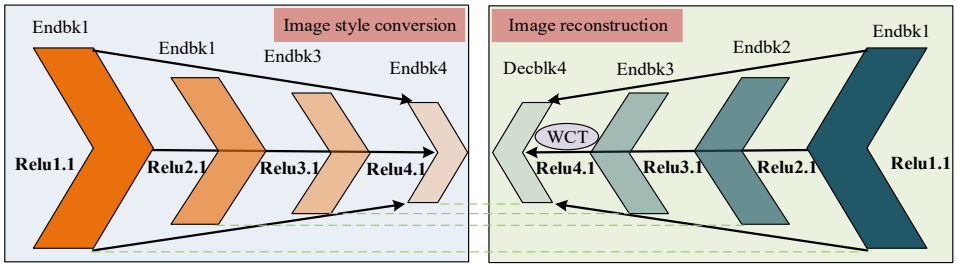

Figure 4. Structure of PhotoWCT image style transfer algorithm

As shown in Figure 4, the PhotoWCT structure consists of two main modules: image style transformation and image reconstruction. The style transformation module follows the whitening and coloring transformation (WCT) process, which removes correlations in the feature map using centering and singular value decomposition. It also adds an orthogonal noise matrix to the whitened features to achieve stylization. The reconstruction module uses a deep learning-based autoencoder to convert coarse-grained features into fine-grained ones. After dimensionality reduction, the decoder reconstructs the original image from the encoded features. During convolutional pooling in the decoder, data loss often occurs. Wavelet pooling helps reduce information loss by decomposing signals into high- and low-frequency components using four convolutional kernels. The calculation of wavelet convolution is shown in Equation 9.

$$\begin{cases} K_{LL}\frac{1}{2}\begin{bmatrix}1 & 1\\ 1 & 1\end{bmatrix} & K_{LH}\frac{1}{2}\begin{bmatrix}-1 & 1\\ -1 & 1\end{bmatrix} \\ K_{HL}\frac{1}{2}\begin{bmatrix}-1 & -1\\ 1 & 1\end{bmatrix} & K_{HH}\frac{1}{2}\begin{bmatrix}1 & -1\\ -1 & 1\end{bmatrix} \end{cases} \tag{9}$$

In Equation 9, K_{LL} and K_{LH} are low-frequency wavelet kernels, while K_{HL} and K_{HH} are high-frequency wavelet kernels. Using skip connections for high-frequency residuals helps reduce the number of convolutional operations and obtain the low-frequency components, as shown in Equation 10.

$$F_{LL}=\left(\frac{1}{2}\begin{bmatrix}1 & 1\\ 1 & 1\end{bmatrix}\square\left(\frac{1}{2}\begin{bmatrix}1 & 1\\ 1 & 1\end{bmatrix}\square F\right)_{\downarrow 2}\right)_{\uparrow 2}=upsampling(avgpooling(F)) \tag{10}$$

In Equation 10, F, $\uparrow 2$, and $\downarrow 2$ represent the feature map, transposed convolution, and convolution, respectively. The high-frequency component is calculated based on the low-frequency part, as shown in Equation 11.

$$F_{LL,HL,HH}=F-F_{LL}=F_{hres}=F-upsampling(avgpooling(F)) \tag{11}$$

In Equation 11, F_{hres} is the high-frequency component obtained via deconvolution. By combining high- and low-frequency components, the original signal is reconstructed to produce better style transfer results. However, the mean and covariance operations in PhotoWCT result in uniformly distributed style transfer, lacking the ability to perform

differentiated style adjustments based on semantics. The Channel Attention Mechanism (CAM) models the channel dimension of input features and adaptively adjusts each channel's response to highlight important information in the image. This balances stylization and intensity [25]. Based on this, the study improves CAM by proposing a Frequency-Separated Channel Attention Mechanism (FS-CAM) to optimize PhotoWCT in performing differentiated style transfer for Zhuang brocade. The operation flow of FS-CAM is shown in Figure 5.

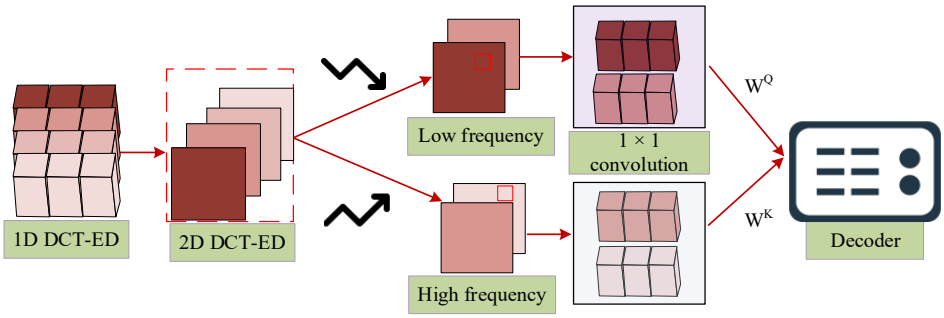

Figure 5. Operation process of FS-CAM attention mechanism

As shown in Figure 5, FS-CAM is built upon the CAM framework and uses Discrete Cosine Transform Eigenvalue Decomposition (DCT-ED) to decompose the initial features. It performs multi-channel parallel filtering on signals with different frequency intensities. Channels with larger coefficients are enhanced, while those with smaller ones are suppressed. This strengthens important feature representation and enables adaptive adjustment for differentiated style transfer. FS-CAM generally performs a discrete cosine transform in two dimensions. The one-dimensional calculation method is shown in Equation 12.

$$f_k = \sum_{i=0}^{L-1} x_i \cos\left(\frac{\pi k}{l}(i+\frac{1}{2})\right) \quad s,t,k \in \{0,1,...,L-1\} \tag{12}$$

In Equation 12, f_k is the DCT-ED frequency spectrum, while F_{hres} and l represent the input value and length. The two-dimensional DCT-ED transformation is shown in Equation 13.

$$f^{2d} = \sum_{i=0}^{H-1}\sum_{j=0}^{W-1} x^{2d} \cos\left(\frac{\pi h}{H}(i+\frac{1}{2})\right)\cos\left(\frac{\pi w}{W}(j+\frac{1}{2})\right) \tag{13}$$

In Equation 13, f^{2d} is the two-dimensional frequency spectrum, x^{2d} is the input of feature map. The corresponding inverse transformation is expressed in Equation 14.

$$Freqi = 2DDCT - EDTi(x^{2d}) = \sum_{h=0}^{H-1}\sum_{w=0}^{W-1} x \, {}^{2d}_{h,w} B \, {}^{i}_{h,w} \tag{14}$$

In Equation 14, $2DDCT$ represents the 2D DCT decomposition of cosine-related variables. The two-dimensional transformation in FS-CAM refines frequency components, allowing precise style transfer on Zhuang brocade textures and tones and enhancing the expression of feature differences. The PhotoWCT algorithm with FS-CAM enhancement, named AM-PWCT, operates as shown in Figure 6.

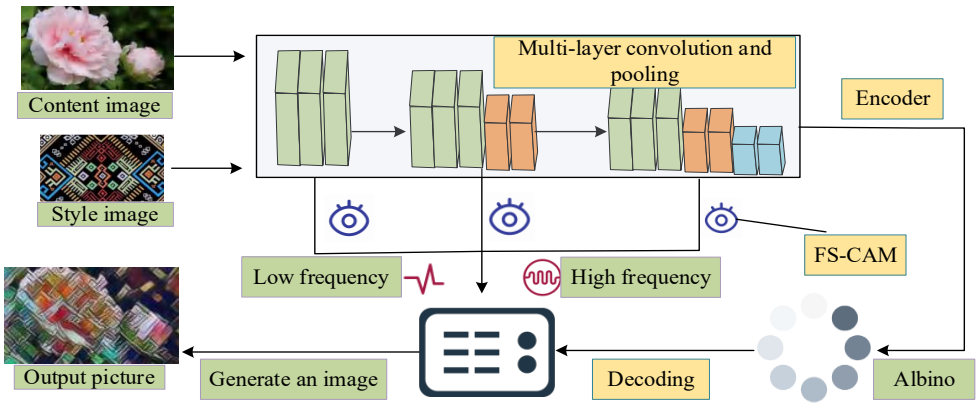

Figure 6. Operation process of AM-PWCT image style transfer algorithm

As shown in Figure 6, AM-PWCT performs style transfer in three stages: encoding convolution, whitening-coloring transformation, and decoding. FS-CAM is embedded in the decoding stage, where it decomposes initial features and sends low- and high-frequency components to the decoder through parallel channels. During this process, the whitening module aligns the covariance of the content image with that of the style image. Finally, the decoder restores the signal and outputs the transferred image. A loss function is constructed to improve the decoder's reconstruction performance. The AM-PWCT loss function is defined in Equation 15.

$$Ltotal = \Psi_{N\neq 1}\left|\phi_{N-1}(I) - decblk_N(\phi_N(I))\right|_2^2 + \lambda\left|\phi_N(I) - \Psi_N(\phi_N(I))\right|_2^2 \tag{15}$$

In Equation 15, ϕ_N represents the encoder-related function, Ψ_N represents the decoder-related function, and λ is the loss coefficient. Training FS-CAM with this loss function increases the attention weight on important image features, enabling more accurate style representation. The function calculation is shown in Equation 16.

$$L_{style} = \frac{1}{4N_l^2 M_l^2}\sum_{l=0}^{4} w_N \sum_{i,j}(G - A)^2 \tag{16}$$

In Equation 16, w_N denotes the encoder's weight parameters, and G and A represent the generated image and its style feature matrix $Gram$. AM-PWCT enhances the overall performance of style transfer by training the decoder and attention module using a style loss function. The Zhuang brocade image generation model combining SD3-GAN and AM-PWCT, referred to as SDGAN-WCT, operates as shown in Figure 7.

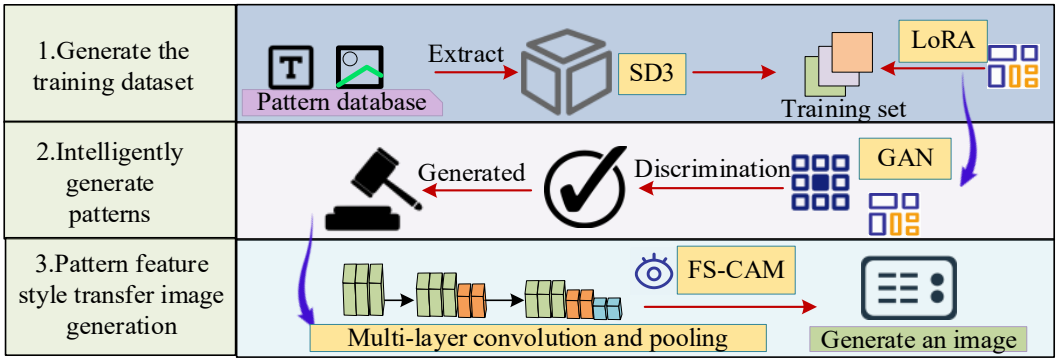

Figure 7. Operation process of the SDGAN-WCT model

As shown in Figure 7, the model integrates the pattern generation capability of SD3-GAN with the style transfer performance of AM-PWCT. The process involves three main steps to generate high-quality Zhuang brocade style images. First, features are extracted from the Zhuang brocade pattern library, and SD3 with LoRA fine-tuning generates the training set for GAN. Then, the generator and discriminator in GAN perform adversarial learning to correct generation logic and produce well-styled patterns. Finally, multi-layer convolution and pooling extract features, FS-CAM focuses on key pattern features, and AM-PWCT assists in performing precise style transfer of the Zhuang brocade patterns.

3. Results

3.1. SD3-GAN-Based Intelligent Generation Test for Zhuang Brocade Patterns

To verify the performance of SD3-GAN, this study used 800 pattern images from the Zhuang brocade library (https://mp.weixin.qq.com/s/1yw3DHtx6qBAX5fkQmMasw) as the dataset and compared it with other pattern generation models, including GAN, Vector Quantized-Variational Autoencoder (VQ-VAE), and OpenAI's second-generation image generation system (DALL-E 2). All experiments were conducted in an environment with Ubuntu 18.04, Python 3.6, RTX 4090 GPU, and AMD Ryzen CPU. The learning rate for all algorithms was set to 0.0001. The comparative results of the Receiver Operating Characteristic (ROC) curve and Area Under the Curve (AUC) among the models are shown in Figure 8.

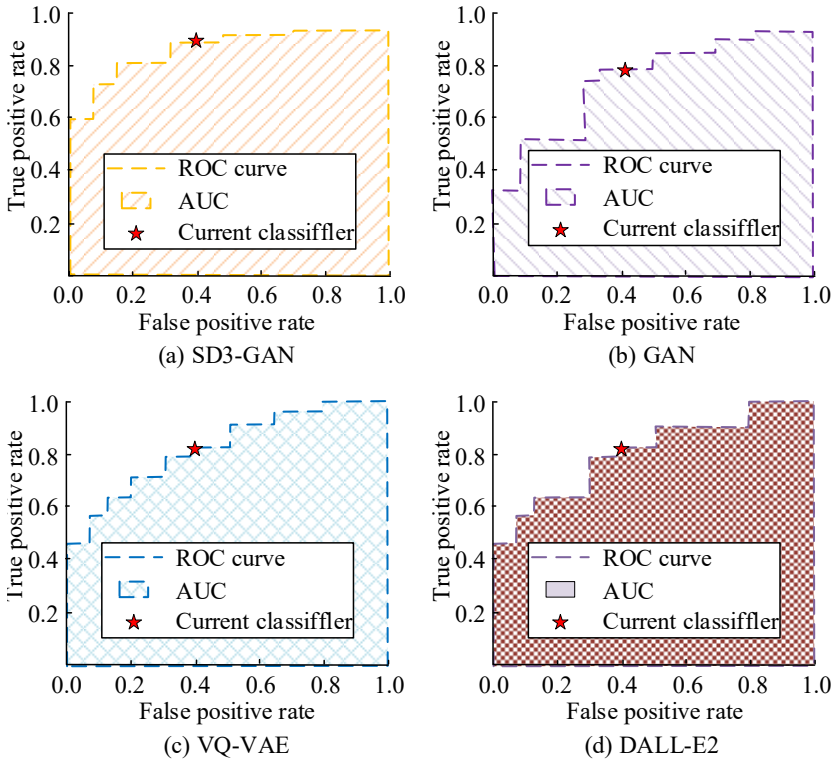

Figure 8. ROC and AUC curve comparisons of different models

As shown in Figure 8(a), the ROC curve of SD3-GAN was clearly convex toward the top-left corner, with an AUC of 0.94. In Figure 8(b), the ROC curve of GAN showed a slight convex trend, but the overall true-positive detection was poor when the false-positive rate was below 0.4, resulting in an AUC of 0.82. Figure 8(c) showed that the ROC curve of VQ-VAE also leaned toward the top-left, with an AUC of 0.84. When the false-positive rate was 0.4, the true-positive rate reached 0.80, indicating good classification performance. In Figure 8(d), the AUC value of DALL-E 2 was 0.85, slightly lower than that of the proposed model. These results demonstrated that SD3-GAN performed best in distinguishing pattern details and structural coherence. The comparison further confirmed the advantage of the image-to-image mechanism in capturing niche features of Zhuang brocade through GAN. SD3-GAN's optimal performance can be attributed to its combination of LoRA's refined feature extraction mechanism and GAN's adversarial training strategy, effectively enhancing its ability to capture and reconstruct the cultural features of Zhuang brocade. As a result, it significantly outperforms existing models in pattern detail resolution and structural consistency. To evaluate the model's robustness in generating Zhuang brocade patterns, the study measured and compared the Peak Signal-to-Noise Ratio (PSNR) under different levels of Gaussian noise. The results are presented in Table 1.

Table 1. PSNR values and confidence intervals under different levels of Gaussian noise

Model	Gaussian Noise (dB)	Average value (dB)	PSNR (dB)		
			85% confidence	90% confidence	95% confidence
SD3-GA	10	32.5	[32.2, 32.8]	[32.0, 33.0]	[31.8, 33.2]
	20	35.2	[35.0, 35.4]	[34.8, 35.6]	[34.6, 35.8]
	30	38.0	[37.8, 38.2]	[37.6, 38.4]	[37.4, 38.6]
VQ-VAE	10	25.3	[24.8, 25.8]	[24.5, 26.1]	[24.2, 26.4]
	20	27.8	[27.3, 28.3]	[27.0, 28.6]	[26.7, 28.9]
	30	30.5	[30.0, 31.0]	[29.7, 31.3]	[29.4, 31.6]
GAN	10	23.6	[23.0, 24.2]	[22.7, 24.5]	[22.4, 24.8]
	20	26.1	[25.5, 26.7]	[25.2, 27.0]	[24.9, 27.3]
	30	28.8	[28.2, 29.4]	[27.9, 29.7]	[27.6, 30.0]
DALL-E2	10	26.8	[26.3, 27.3]	[26.0, 27.6]	[25.7, 27.9]
	20	29.5	[29.0, 30.0]	[28.7, 30.3]	[28.4, 30.6]
	30	32.2	[31.7, 32.7]	[31.4, 33.0]	[31.1, 33.3]

In Table 1, when the Gaussian noise was set to 10 dB, the average PSNR values of SD3-GAN, VQ-VAE, GAN, and DALL-E 2 were 32.5 dB, 25.3 dB, 23.6 dB, and 26.8 dB, respectively. Their 95% confidence intervals were [31.8 dB, 33.2 dB], [24.2 dB, 26.4 dB], [22.4 dB, 24.8 dB], and [25.7 dB, 27.9 dB], respectively. Further analysis under 20 dB and 30 dB of Gaussian noise showed the same trend—SD3-GAN consistently produced higher average PSNR with narrower intervals and higher lower bounds. The results indicate that SD3-GAN has the highest average PSNR and the narrowest confidence interval in the intelligent generation of Zhuang brocade patterns, demonstrating excellent robustness and adaptability. This result fully demonstrates that the proposed SD3-GAN model has excellent robustness in terms of noise resistance and pattern structure restoration, and is more suitable for the high fidelity generation needs of complex cultural patterns such as Zhuang brocade. Zhuang brocade contains complex patterns such as “double phoenix facing the sun,” “phoenix through peony,” “two dragons playing with a pearl,” and “lion rolling embroidered ball.” These are among the most intricate pattern types. The feature recognition performance of different models on these complex patterns was simulated through clustering, as shown in Figure 9, where red represents the double phoenix, yellow the phoenix through peony, purple the dragons, and brown the lion pattern.

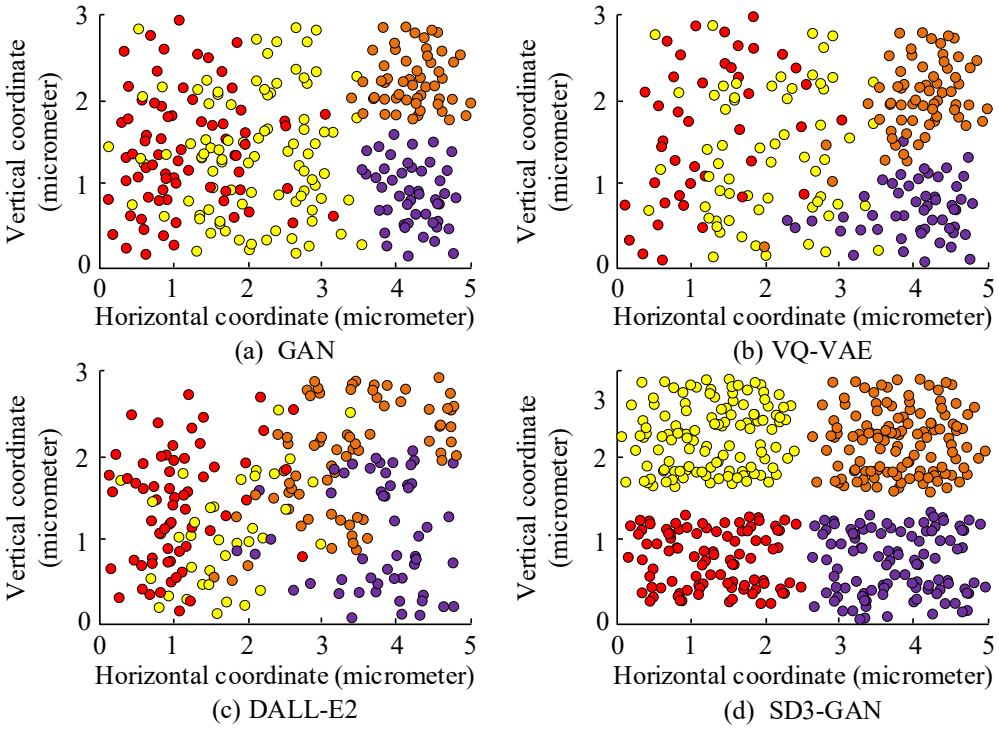

Figure 9. Comparison of complex pattern feature recognition

In Figure 9(a), the four types of data points were heavily overlapped with no clear clustering boundaries, indicating GAN's lack of capability in structured analysis of cultural pattern features. In Figure 9(b), the yellow points were scattered within clusters, and interclass overlap between yellow and red points was still visible, suggesting loose clustering. Figure 9(c) showed some separation between red and yellow clusters, but purple and brown still overlapped, reflecting limited class differentiation. DALL-E 2's general pretraining failed to capture specific cultural features of Zhuang brocade. In contrast, Figure 9(d) displayed compact and distinct clusters with clear boundaries and high intra-class cohesion. These results showed that the image-to-image generation mechanism, based on training with generated datasets, enabled the proposed model to better capture the structural hierarchy, cultural symbols, and craftsmanship logic of Zhuang brocade. Its feature recognition ability significantly outperformed traditional models.

3.2. Practical Performance Validation of the SDGAN-WCT Model

After confirming the model's effectiveness in pattern generation, the study further evaluated its style transfer performance by comparing it with Neural Style Transfer (NST), Style Generative Adversarial Network (StyleGAN), and StyleFormer. A group of images from the dataset was used for style transfer by each model, and the average Structural Similarity Index (SSIM) at different image regions was compared, as shown in Figure 10.

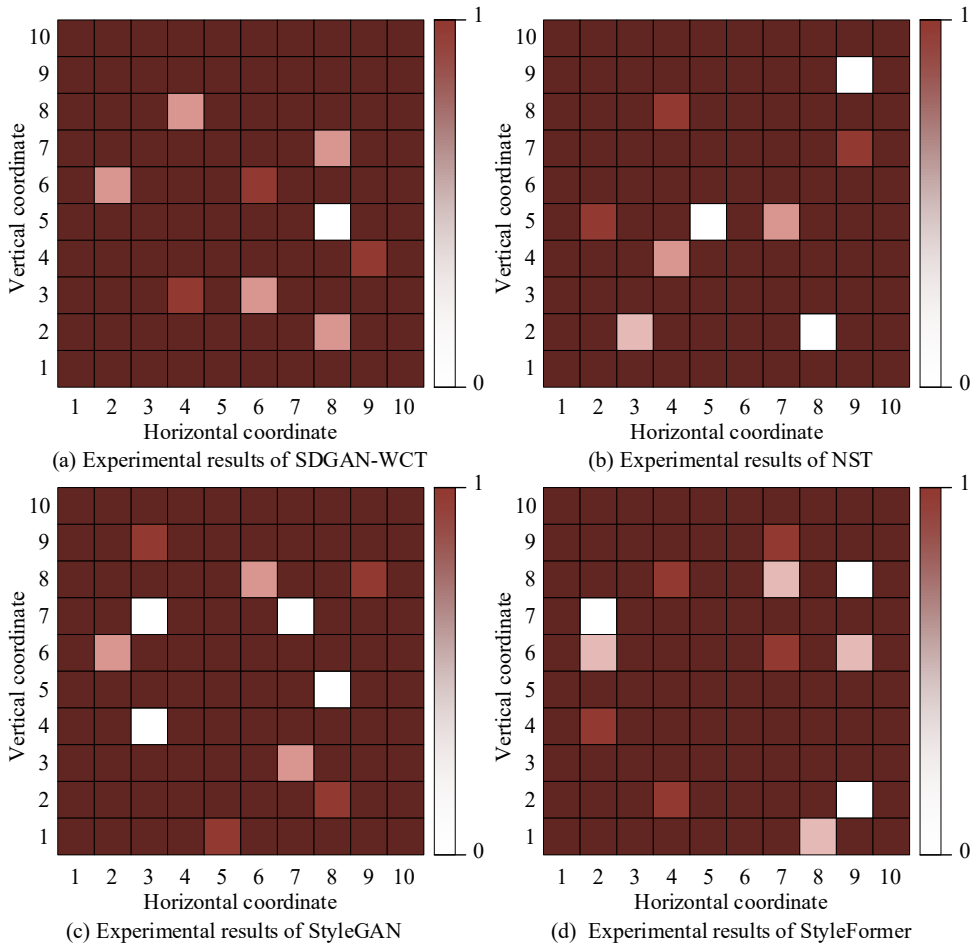

Figure 10. SSIM value comparison of different models across image regions

As shown in Figure 10(a), 92% of the regions in the image generated by SDGAN-WCT had an SSIM value of 1.0. In Figure 10(b), the NST-transferred image had 87% of its regions at SSIM 1.0. In Figure 10(c), StyleGAN achieved 89%, and Figure 10(d) showed that StyleFormer reached only 77%, all significantly lower than SDGAN-WCT. Moreover, in the SDGAN-WCT image, only 4% of regions had an SSIM of 0, and the overall distribution was more balanced. The results indicate that SDGAN-WCT has high integrity and consistency in restoring structural and color features, mainly due to the introduction of FS-CAM, which explicitly separates and enhances low-frequency structures and high-frequency detail features through discrete cosine transform, preserving the key cultural symbol structures and textures of the content image during style transfer. To assess the model's ability to transfer styles of complex Zhuang patterns, the study applied the models to three representative styles: “double phoenix facing the sun,” “phoenix through peony,” and “two dragons playing with a pearl” (referred to as 1, 2, and 3 for simplicity). The Inception Score (IS) and Coverage-Diversity Score (CD Score) of the transferred images were statistically compared, as shown in Figure 11.

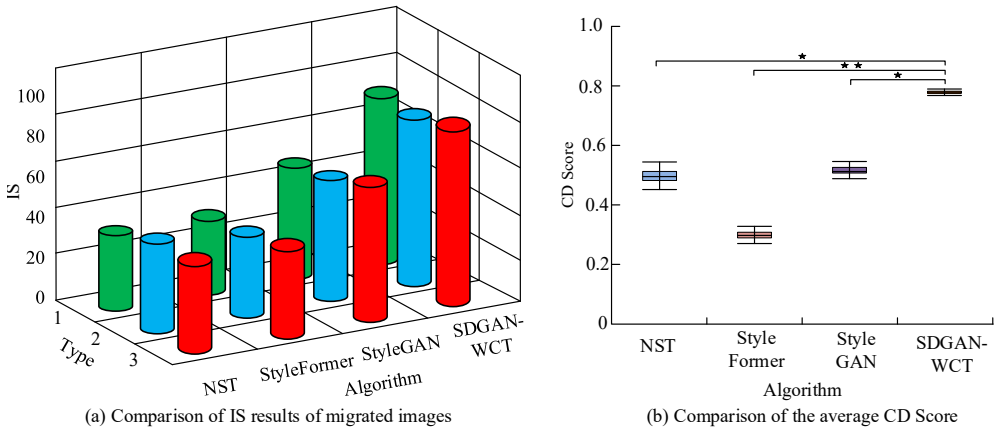

Figure 11. Statistical metric comparison for style transfer

In Figure 11(a), SDGAN-WCT achieved IS scores of 78.3, 80.1, and 81.1 for the three patterns. In contrast, NST obtained scores of 58.9, 61.1, and 63.3, while the average IS score of StyleGAN was 40.2, higher than StyleFormer's average of 39.5. These results indicated that SDGAN-WCT offered better diversity and semantic extraction, resulting in higher image quality. In Figure 11(b), SDGAN-WCT achieved an average CD score of 0.78, significantly higher than NST (0.57), StyleGAN (0.35), and StyleFormer (0.56). Additionally, SDGAN-WCT's CD scores were more concentrated. The results indicate that the stylization results of the SDGAN-WCT model have significant advantages in covering different local features and maintaining structural diversity. This is because the FS-CAM in the model effectively coordinates the global consistency constraints and local feature variability in style transfer, thereby generating rich and high fidelity pattern variants while preserving the essence of cultural symbols. The study also compared the memory usage and response time under varying data volumes, as shown in Figure 12.

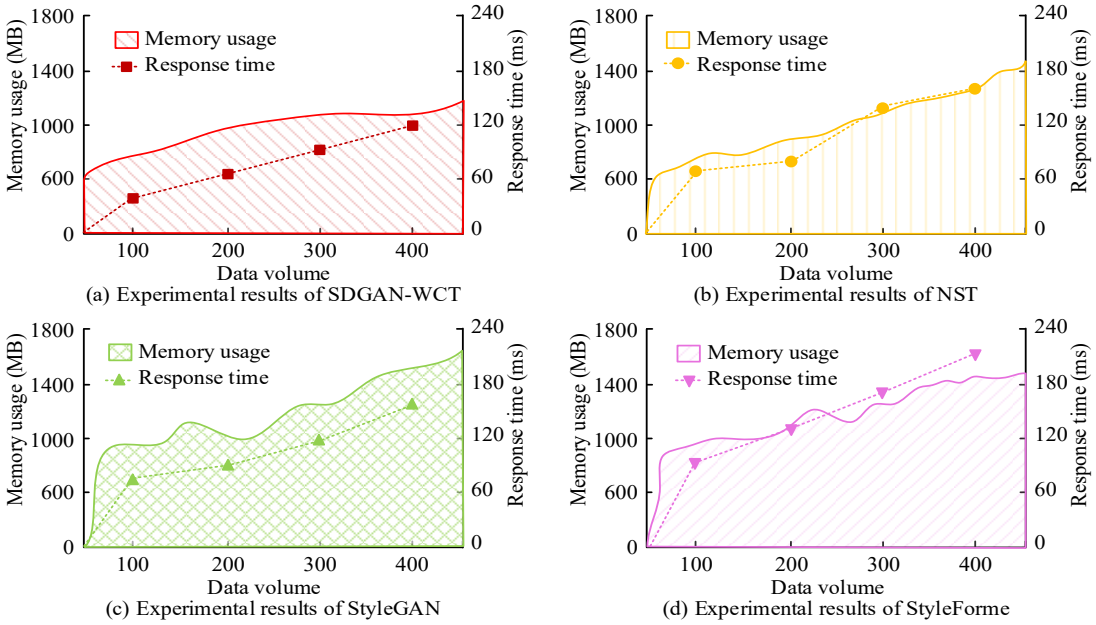

Figure 12. Comparison of memory usage and response time across models

As shown in Figure 12(a), SDGAN-WCT exhibited stepwise memory growth and linear response time increases, both with relatively low growth rates. When the data volume reached 40, memory usage was 1123 MB, and response time was 122 ms. In Figure 12(b), NST's memory usage grew steadily, while its response time increased slowly at first, then more quickly, reaching 185 ms. Figure 12(c) showed that StyleGAN's response time grew rapidly with fluctuations, and its memory and time usage spiked in later stages, showing the highest resource consumption. In Figure 12(d), StyleFormer's final memory usage and response time were 1379 MB and 225 ms, respectively. These results indicated that SDGAN-WCT maintained efficient performance under increasing data volume, offering better lightweight performance than the other models. The model's efficient resource utilization mainly stems from its adoption of the LoRA lightweight fine-tuning strategy, which significantly reduces the number of trainable parameters through low-rank decomposition, avoiding the computational burden of full model fine-tuning. At the same time, combined with the adversarial optimization of GAN and the focused computation of the FS-CAM module, it effectively reduces redundant feature extraction and iteration, thus maintaining low memory usage and stable computational efficiency when scaling to large datasets. To evaluate real-world style transfer performance, the study applied the models to practical Zhuang brocade patterns, including the Wanzi chrysanthemum pattern and Binyang brocade from Guangxi. The results are shown in Figure 13.

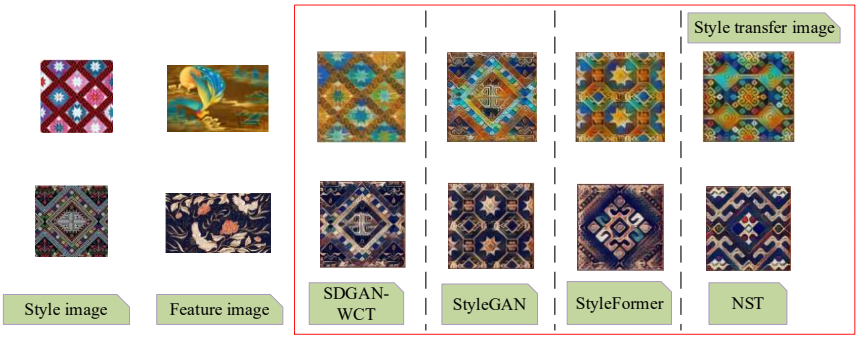

Figure 13. Real-world image comparisons of style transfer across models

As shown in Figure 13, SDGAN-WCT accurately replicated the color gradation and pattern details of the style images, while preserving the structural texture of the content images. The generated patterns were neat and clear with harmonious color transitions. In comparison, StyleGAN suffered from blurred textures, and StyleFormer exhibited harsh color blending. These results demonstrated that SDGAN-WCT achieved superior visual balance between style and content, making it more aesthetically effective for traditional brocade style transfer. To further validate the superiority of the proposed SDGAN-WCT model, it was compared with three currently advanced style transfer models, DALL-E 3, SD3, and Wuerstchen v2. This study used Cultural Symbol Accuracy (CSA), Structural Similarity (SSIM), and Aesthetic Score (AS) as evaluation metrics for cultural symbol recognition. CSA measures cultural semantic preservation ability by calculating the matching degree between generated images and a series of Zhuang cultural symbol text descriptions using a CLIP model. The SSIM metric can evaluate the structural consistency between generated images and content images. The aesthetic score is based on a Large-scale Artificial Intelligence Open Network pre-trained model to evaluate the visual aesthetics of images. The comparison results of the indicators of the four models are shown in Table 2.

Table 2. Comparison results of indicators for four models

Models	CSA	SSIM	AS
DALL-E 3	0.74	0.88	6.85
SD3	0.67	0.83	6.44
Wuerstchen v2	0.69	0.81	6.59
SDGAN-WCT	0.91	0.90	7.06

From Table 2, it can be seen that the proposed SDGAN-WCT model performs the best in CSA, SSIM, and AS indicators, with scores of 0.91, 0.90, and 7.06, respectively. This is mainly due to LoRA's targeted fine-tuning of Zhuang cultural characteristics and the semantic protection mechanism of FS-CAM module, which enables SDGAN-WCT to most effectively preserve the core cultural symbols and structural features of patterns in the generation and transformation process. However, the SD3 and Wuerstchen v2 models perform poorly in cultural adaptation tasks without targeted optimization. In summary, the SDGAN-WCT model has unique and significant advantages over the latest general diffusion models in maintaining cultural symbol accuracy and structural authenticity. Finally, in order to subjectively evaluate the results of the style transition, this study invited three groups of 60 participants (20 people in each group) with different levels of familiarity with Zhuang culture to participate in the evaluation: Group A is an expert in Zhuang textile and cultural heritage research; Group B is a designer engaged in related work; and Group C is an ordinary user. The evaluation adopts a blind test format, requiring participants to rate the results generated by different models from three dimensions: aesthetic attractiveness, pattern regularity, and style similarity. The results are presented in Table 3.

Table 3. Comprehensive evaluation of preference for transferred images across models

Indicator	Rating level	SDGAN-WCT	NST	StyleGAN	StyleFormer
Artistic aesthetic appeal	The highest	65%	30%	45%	20%
	Medium	25%	45%	35%	35%
	The lowest	10%	25%	20%	45%
The standardization of the pattern	The highest	60%	45%	35%	15%
	Medium	30%	35%	40%	30%
	The lowest	10%	20%	25%	55%
Style similarity	The highest	66%	35%	38%	12%
	Medium	28%	45%	42%	25%
	The lowest	6%	20%	20%	63%

As shown in Table 3, SDGAN-WCT received the highest proportion (65%) in aesthetic appeal, surpassing NST (30%), StyleGAN (45%), and StyleFormer (20%), confirming its visual superiority. In terms of pattern regularity, SDGAN-WCT had the lowest negative rating at only 10%, indicating precise feature extraction and structured transfer. Regarding style similarity, NST had a moderate rating (45%), while SDGAN-WCT achieved the highest overall approval rating at 94%. These results indicate that the proposed model outperforms the others in aesthetics, structural consistency, and stylistic resemblance.

4. Discussion

The proposed SDGAN-WCT model demonstrated significant advantages in the tasks of intelligent generation and style transfer of Zhuang brocade patterns. Its performance was consistent with existing studies and also demonstrated innovative breakthroughs. This section analyzes the model in terms of generation robustness, style transfer precision, resource efficiency, and feature learning capability. In terms of robustness, the SD3-GAN model achieved significantly higher PSNR under various levels of Gaussian noise compared to other models. At 10 dB noise, its average PSNR reached 32.5 dB, which was much higher than GAN (23.6 dB), VQ-VAE (25.3 dB), and DALL-E 2 (26.8 dB). The 95% confidence interval was also narrower, at [31.8, 33.2], indicating the model's ability to consistently generate high-quality Zhuang patterns even under noise. This result confirmed the critical role of the adversarial mechanism in GAN in improving model robustness. Gaber et al. proposed a GAN-based model for IoT attack detection using adversarial training. Their approach enhanced the model's recognition ability for abnormal data through dynamic interaction between the generator and discriminator. This was consistent with the optimization logic of SD3-GAN in this study, where adversarial training improved the model's adaptability to noise or abnormal features [26].

However, while Gaber et al. focused on robustness in classification tasks, this study applied the GAN mechanism to image generation. The discriminator provided corrective feedback on pattern details and structure, addressing blurriness and deviation in SD3's initial outputs and producing clearer clustering boundaries for complex patterns [26]. These results suggested that the adversarial mechanism not only improved robustness in visual generation tasks but also enhanced the model's ability to structurally interpret cultural symbols. With the combined effect of the attention mechanism and frequency separation, SDGAN-WCT achieved excellent style transfer performance, as reflected in SSIM, IS, and CD scores. It produced images where 92% of the regions had an SSIM value of 1.0, which was significantly higher than NST (87%), StyleGAN (89%), and StyleFormer (77%). For the “double phoenix facing the sun” pattern, the model achieved an IS value of 81.1 and a CD score of 0.78, indicating that the transferred results preserved the structural integrity of Zhuang patterns while achieving diverse style expression. This result aligned with Moon et al.'s MIST-Tacotron model, which achieved emotional speech synthesis through mel-spectrogram style transfer. Its core logic of preserving emotional features via feature decomposition was highly consistent with the FS-CAM mechanism proposed in this study [27]. Compared with the ArtBank framework proposed by Zhang et al. [7], this research method not only maintains higher visual authenticity (SSIM of 0.92) in the process of style transfer, but also effectively preserves the unique cultural symbol features of Zhuang brocade by introducing a semantic perception module, solving the shortcomings of ArtBank in the transfer of specific ethnic cultural elements. In addition, compared to Yan et al.'s GAN based texture understanding entanglement method [8], this model adopts a strategy combining LoRA fine-tuning and adversarial training, which performs better in generating patterns with structural coherence (PSNR 32.5 dB) and diversity (CD Score 0.78), especially in dealing with multi-level features of complex ethnic patterns.

The SDGAN-WCT model also showed excellent resource stability when handling increasing data volume. At a data volume of 400, it only occupied 1123 MB of memory and required 122 ms response time, which was significantly lower than StyleGAN and StyleFormer (225 ms). This advantage came from the application of LoRA, which fine-tuned only 1% of the SD3 model's parameters via low-rank matrix decomposition, and the AM-PWCT algorithm, which reduced convolution operations through wavelet pooling and high-frequency residual skip connections. MobileAR-GAN used the lightweight MobileNet architecture to improve efficiency, while this study reduced resource consumption by parameter decomposition without compromising model capacity [28]. The SD3-GAN model also achieved excellent performance in recognizing features of complex compound Zhuang patterns. In the clustering experiments involving four pattern types—”double phoenix facing the sun,” “phoenix through peony,” “two dragons playing with a pearl,” and “lion rolling embroidered ball”—the model produced compact and well-separated feature clusters, indicating a stronger ability to capture cultural symbols in Zhuang brocade, such as the meanings of animal motifs and the arrangement logic of geometric patterns. This finding echoed the work of Jimale et al. who highlighted the incremental adaptability of GAN in feature learning and how a fully connected GAN could iteratively learn dynamic features of human activities. Similarly, incremental training with defected samples enabled the SD3-GAN model to gradually learn the hierarchical structure of Zhuang brocade patterns [29]. The comparative data analysis showed that the SD3-GAN model achieved an AUC of 0.94, indicating superior ability in distinguishing pattern details and structural coherence. This result extended the application scenarios of GAN incremental learning as emphasized by Behara et al. and Singh et al. demonstrating its potential in cultural heritage generation tasks that contain highly specific features. It also proved GAN's ability to compensate for the limitations of general models in such domains [30, 31].

By integrating LoRA, GAN, and an improved style transfer algorithm, this study verified the collaborative effectiveness of low-rank adaptation, adversarial learning, and attention mechanisms in the tasks of generating and transferring Zhuang brocade patterns. In practical applications, the proposed SDGAN-WCT model demonstrated good transferability and can provide a universal solution for the digital protection and innovation of other types of intangible cultural heritage (ICH). For example, for the geometric patterns and color systems of Uyghur carpets, or the totem symbols and composition rules of Miao embroidery, simply replacing the corresponding training dataset and constructing its unique cultural symbol text library, this framework can also perform high-quality intelligent generation and style adaptation. Therefore, this study not only provides an effective technical solution for pattern generation and style transformation of Zhuang brocade but also establishes a digital innovation framework for cultural heritage that is adaptable to different cultural contexts and aligns with sustainable development goals.

5. Conclusion

To address the problems of low design efficiency and stylistic mismatch with modern demands in Zhuang brocade pattern design, this study built an SDGAN-WCT model for intelligent generation and style transfer of Zhuang patterns. The overall performance showed significant advantages. In the generation stage, the model used LoRA to perform low-rank adaptation on SD3, which effectively reduced resource consumption during large model training. At the same time, it enhanced the model's ability to capture niche features of Zhuang brocade. By incorporating the adversarial mechanism of GAN, the model applied a degradation-driven image-to-image generation process to overcome the limitations of general generation models in interpreting cultural features. In the style transfer stage, the model improved PhotoWCT through the FS-CAM mechanism. This enabled differentiated style adaptation for various semantic units in the Zhuang patterns and avoided the uniform transfer problem of traditional algorithms. As a result, the transferred patterns could better align with modern product design contexts while preserving the cultural essence of the original motifs. The technical framework proposed in this study has clear practical application value and broad prospects. It can not only be used for digital archiving and innovative design of Zhuang brocade, but also promoted to the modernization transformation of other ethnic intangible cultural heritage artworks, such as Miao embroidery and Tibetan carpets. In practical applications, the proposed model can effectively support the development of cultural and creative products, personalized customized clothing, and the construction of cultural and tourism IP through lightweight and high fidelity generation and transfer capabilities. In addition, by further optimizing textile process parameters, the model is expected to be integrated into intelligent manufacturing processes, ensuring that the patterns generated by the model can be directly used for production, thereby promoting the sustainable inheritance and industrialization of traditional culture in the digital economy.

In summary, the main advantage and innovation of this study lies in proposing a hybrid pattern generation and style transfer model that integrates LoRA, improved GAN, attention mechanism, and PhotoWCT. This model first achieves efficient extraction and adaptation of cultural features through LoRA, and then combines improved GAN to enhance the structural authenticity and detail richness of generated patterns. FS-CAM is introduced to achieve semantic guided style transfer, which significantly reduces the computational resource requirements while effectively solving the problems of cultural feature loss, poor style adaptability, and semantic inconsistency commonly found in traditional methods for ethnic pattern generation. It provides a scalable technical path for the digital protection and innovation of intangible cultural heritage. However, this study still has certain limitations. First, semantic adaptation in style transfer mainly relies on visual feature matching and lacks the ability to respond to implicit design needs of specific product contexts. The current approach could not fully meet such nuanced demands. Secondly, the model training relies on a single ethnic pattern dataset, and its cross-cultural generalization ability has not been verified. Therefore, in future research, the text description of product scenarios should be further integrated into the decision-making process to improve the accuracy of cultural adaptation and further expand the application of this model in the digital preservation and dissemination of intangible cultural heritage. In addition, a multi-ethnic intangible cultural heritage pattern dataset will be constructed, and a pluggable LoRA adapter will be used to achieve on-demand switching of different cultural characteristics.

6. Declarations

6.1. Author Contributions

L.Z. and X.N. contributed to the design and implementation of the research, to the analysis of the results and to the writing of the manuscript. All authors have read and agreed to the published version of the manuscript.

6.2. Data Availability Statement

The data presented in this study are available on request from the corresponding author.

6.3. Funding

The authors received no financial support for the research, authorship, and/or publication of this article.

6.4. Institutional Review Board Statement

Not applicable.

6.5. Informed Consent Statement

Not applicable.

6.6. Declaration of Competing Interest

The authors declare that they have no known competing financial interests or personal relationships that could have appeared to influence the work reported in this paper.

7. References

[1] Wang, X., Yang, S., Wang, W., & Liu, J. (2022). Artistic Text Style Transfer: An overview of state-of-the-art methods and datasets [SP Forum]. IEEE Signal Processing Magazine, 39(6), 10–17. doi:10.1109/MSP.2022.3196763.

[2] Psychogyios, K., Leligou, H. C., Melissari, F., Bourou, S., Anastasakis, Z., & Zahariadis, T. (2023). SAMStyler: Enhancing Visual Creativity with Neural Style Transfer and Segment Anything Model (SAM). IEEE Access, 11, 100256–100267. doi:10.1109/ACCESS.2023.3315235.

[3] Cotogni, M., Arazzi, M., & Cusano, C. (2024). PhotoStyle60: A Photographic Style Dataset for Photo Authorship Attribution and Photographic Style Transfer. IEEE Transactions on Multimedia, 26, 10573–10584. doi:10.1109/TMM.2024.3408683.

[4] Khan, O. S., Iltaf, N., Zia, U., Latif, R., & Jamail, N. S. M. (2024). Efficient Text Style Transfer Through Robust Masked Language Model and Iterative Inference. IEEE Access, 12, 182353–182373. doi:10.1109/ACCESS.2024.3501320.

[5] Moar, C., Tahmasebi, F., Pellauer, M., & Kwon, H. (2024). Characterizing the Accuracy-Efficiency Trade-off of Low-rank Decomposition in Language Models. 2024 IEEE International Symposium on Workload Characterization (IISWC), 194–209. doi:10.1109/IISWC63097.2024.00026.

[6] Mao, W., Yang, S., Shi, H., Liu, J., & Wang, Z. (2023). Intelligent Typography: Artistic Text Style Transfer for Complex Texture and Structure. IEEE Transactions on Multimedia, 25(2), 6485–6498. doi:10.1109/TMM.2022.3209870.

[7] Zhang, Z., Zhang, Q., Xing, W., Li, G., Zhao, L., Sun, J., Lan, Z., Luan, J., Huang, Y., & Lin, H. (2024). ArtBank: Artistic Style Transfer with Pre-trained Diffusion Model and Implicit Style Prompt Bank. Proceedings of the AAAI Conference on Artificial Intelligence, 38(7), 7396–7404. doi:10.1609/aaai.v38i7.28570.

[8] Yan, H., Zhang, H., Shi, J., Ma, J., & Xu, X. (2023). Inspiration Transfer for Intelligent Design: A Generative Adversarial Network With Fashion Attributes Disentanglement. IEEE Transactions on Consumer Electronics, 69(4), 1152–1163. doi:10.1109/TCE.2023.3255831.

[9] Liu, M., Zhu, A. H., Maiti, P., Thomopoulos, S. I., Gadewar, S., Chai, Y., Kim, H., & Jahanshad, N. (2023). Style transfer generative adversarial networks to harmonize multisite MRI to a single reference image to avoid overcorrection. Human Brain Mapping, 44(14), 4875–4892. doi:10.1002/hbm.26422.

[10] Garg, M., Ubhi, J. S., & Aggarwal, A. K. (2023). Neural style transfer for image steganography and destylization with supervised image to image translation. Multimedia Tools and Applications, 82(4), 6271–6288. doi:10.1007/s11042-022-13596-3.

[11] Wang, Z., Zhou, Y., Shi, Y., & Letaief, K. B. (2024). Federated Low-Rank Adaptation for Large Language Model Fine-Tuning Over Wireless Networks. Proceedings - IEEE Global Communications Conference, GLOBECOM, 20(3), 3063–3068. doi:10.1109/GLOBECOM52923.2024.10901572.

[12] Jin, F., Liu, Y., & Tan, Y. (2024). Derivative-Free Optimization for Low-Rank Adaptation in Large Language Models. IEEE/ACM Transactions on Audio Speech and Language Processing, 32, 4607–4616. doi:10.1109/TASLP.2024.3477330.

[13] Imam, R., Gani, H., Huzaifa, M., & Nandakumar, K. (2025). Test-Time Low Rank Adaptation via Confidence Maximization for Zero-Shot Generalization of Vision-Language Models. 2025 IEEE/CVF Winter Conference on Applications of Computer Vision (WACV), 5449–5459. doi:10.1109/WACV61041.2025.00532.

[14] Bechar, A., Elmir, Y., Himeur, Y., Medjoudj, R., & Amira, A. (2024). Enhancing Cancer Detection with Fine-Tuned Large Language Models: A Comparative Study on Low-Rank Adaptation. 2024 IEEE/ACM International Conference on Big Data Computing, Applications and Technologies (BDCAT), 360–365. doi:10.1109/BDCAT63179.2024.00062.

[15] Lu, Y., Wong, W. K., Yuan, C., Lai, Z., & Li, X. (2024). Low-Rank Correlation Learning for Unsupervised Domain Adaptation. IEEE Transactions on Multimedia, 26(11), 4153–4167. doi:10.1109/TMM.2023.3321430.

[16] Mishra, D., & Hadar, O. (2023). Accelerating Neural Style-Transfer Using Contrastive Learning for Unsupervised Satellite Image Super-Resolution. IEEE Transactions on Geoscience and Remote Sensing, 61(4705014), 1–14,. doi:10.1109/TGRS.2023.3314283.

[17] Toshevska, M., & Gievska, S. (2025). LLM-Based Text Style Transfer: Have We Taken a Step Forward? IEEE Access, 13(4), 44707–44721. doi:10.1109/ACCESS.2025.3548967.

[18] Veasey, B. P., & Amini, A. A. (2025). Low-Rank Adaptation of Pre-Trained Large Vision Models for Improved Lung Nodule Malignancy Classification. IEEE Open Journal of Engineering in Medicine and Biology, 6(10), 296–304. doi:10.1109/OJEMB.2025.3530841.

[19] Choi, J., Hong, S., Hong, S., Park, J., & Jung, E. S. (2025). Toward Generating Quality Test Questions and Answers Using Quantized Low-Rank Adapters in LLMs. IEEE Access, 13(2), 87793–87809. doi:10.1109/ACCESS.2025.3570567.

[20] Baby, A., Joseph, G., & Singh, S. (2024). Robust Speaker Personalisation Using Generalized Low-Rank Adaptation for Automatic Speech Recognition. ICASSP 2024 - 2024 IEEE International Conference on Acoustics, Speech and Signal Processing (ICASSP), 11381–11385. doi:10.1109/ICASSP48485.2024.10446630.

[21] Rasheed, I., Asif, M., Ihsan, A., Khan, W. U., Ahmed, M., & Rabie, K. M. (2023). LSTM-Based Distributed Conditional Generative Adversarial Network for Data-Driven 5G-Enabled Maritime UAV Communications. IEEE Transactions on Intelligent Transportation Systems, 24(2), 2431–2446. doi:10.1109/TITS.2022.3187941.

[22] Gupta, C., Das, R. K., Barik, R. K., Qurashi, S. N., Roy, D. S., & Yadav, S. S. (2025). GANCE: Generative Adversarial Network Assisted Channel Estimation for Unmanned Aerial Vehicles Empowered 5G and Beyond Wireless Networks. IEEE Access, 13(10), 198–213. doi:10.1109/ACCESS.2024.3522847.

[23] Preethi, P., & Mamatha, H. R. (2023). Region-Based Convolutional Neural Network for Segmenting Text in Epigraphical Images. Artificial Intelligence and Applications, 1(2), 103–111. doi:10.47852/bonviewAIA2202293.

[24] Tran, V. N., Choi, P., Le, H. S., Lee, S. H., & Kwon, K. R. (2025). DiffCoR: Exposing AI-Generated Image by Using Stable Diffusion Model Based on Consistent Representation Learning. IEEE Open Journal of the Computer Society, 6(10), 1353–1365. doi:10.1109/OJCS.2025.3575507.

[25] Gaber, T., Ali, T., Nicho, M., & Torky, M. (2025). Robust Attacks Detection Model for Internet of Flying Things Based on Generative Adversarial Network (GAN) and Adversarial Training. IEEE Internet of Things Journal, 12(13), 23961–23974. doi:10.1109/JIOT.2025.3555202.

[26] Kim, S., Jang, B., Lee, J., Bae, H., Jang, H., & Park, I.-C. (2023). A CNN Inference Accelerator on FPGA With Compression and Layer-Chaining Techniques for Style Transfer Applications. IEEE Transactions on Circuits and Systems I: Regular Papers, 70(4), 1591–1604. doi:10.1109/TCSI.2023.3234640.

[27] Moon, S., Kim, S., & Choi, Y. H. (2022). MIST-Tacotron: End-to-End Emotional Speech Synthesis Using Mel-Spectrogram Image Style Transfer. IEEE Access, 10(7), 25455–25463. doi:10.1109/ACCESS.2022.3156093.

[28] Yadav, N. K., Singh, S. K., & Dubey, S. R. (2022). MobileAR-GAN: MobileNet-Based Efficient Attentive Recurrent Generative Adversarial Network for Infrared-to-Visual Transformations. IEEE Transactions on Instrumentation and Measurement, 71(10), 1–9. doi:10.1109/TIM.2022.3166202.

[29] Jimale, A. O., & Mohd Noor, M. H. (2022). Fully Connected Generative Adversarial Network for Human Activity Recognition. IEEE Access, 10(2), 100257–100266. doi:10.1109/ACCESS.2022.3206952.

[30] Behara, R. K., & Saha, A. K. (2024). Analysis of Wind Characteristics for Grid-Tied Wind Turbine Generator Using Incremental Generative Adversarial Network Model. IEEE Access, 12(12), 38315–38334. doi:10.1109/ACCESS.2024.3372862.

[31] Singh, B., & Bhuvaneswari, G. (2020). Grid-tied battery integrated wind energy generation system with an ability to operate under adverse grid conditions. IEEE Transactions on Industry Applications, 56(6), 6882-6891. doi:10.1109/TIA.2020.3024156.